Tunable disorder and localization in the rare-earth nickelates

Changan Wang,[1,2,3,*] Ching-Hao Chang,[4,5,†] Angus Huang,[6] Pei-Chun Wang,[7] Ping-Chun Wu,[7] Lin Yang,[8] Chi Xu,[1,2] Parul Pandey,[1] Min Zeng,[8] Roman Böttger,[1] Horng-Tay Jeng,[6,9] Yu-Jia Zeng,[3] Manfred Helm,[1,2] Ying-Hao Chu,[7,10] R. Ganesh,[11] and Shengqiang Zhou[1]

[1]*Helmholtz-Zentrum-Dresden-Rossendorf, Bautzner Landstraße 400, 01328 Dresden, Germany*
[2]*Technische Universität Dresden, 01062 Dresden, Germany*
[3]*Shenzhen Key Laboratory of Laser Engineering, College of Physics and Optoelectronic Engineering, Shenzhen University, 518060 Shenzhen, China*
[4]*Department of Physics, National Cheng Kung University, Tainan 70101, Taiwan*
[5]*Leibniz-Institute for Solid State and Materials Research, Helmholtzstraße 20, 01069 Dresden, Germany*
[6]*Department of Physics, National Tsing Hua University, Hsinchu 30043, Taiwan*
[7]*Department of Materials Science and Engineering, National Chiao Tung University, Hsinchu 30010, Taiwan*
[8]*Institute for Advanced Materials and Guangdong Provincial Key Laboratory of Quantum Engineering and Quantum Materials, South China Normal University, Guangzhou 51006, China*
[9]*Institute of Physics, Academia Sinica, Taipei 11529, Taiwan*
[10]*Center for Emergent Functional Matter Science, National Chiao Tung University, Hsinchu 30010, Taiwan*
[11]*The Institute of Mathematical Sciences, HBNI, CIT Campus, Chennai 600113, India*

(Received 2 July 2018; revised manuscript received 12 December 2018; published 2 May 2019)

We demonstrate that transport in metallic rare-earth nickelates can be engineered by directly tuning the electronic mean free path. Using irradiation as a tool to induce disorder, we drive this system from a metallic phase into an Anderson insulator. This proceeds via an intermediate regime which shows a thermal crossover from insulating to metallic behavior. We argue that this phase falls within the paradigm of weak localization in three dimensions. We develop a theoretical model for the temperature dependence of resistivity which shows good agreement with our data. The three-dimensional weak localization picture is supported by magnetoconductivity, which scales as $\sim B^2$ up to several tesla. Interestingly, our data indicate that this phase lies in the Mott-Ioffe-Regel regime with the mean free path approaching the lattice constant. Upon further increasing disorder, the charge carriers are localized, leading to insulating behavior at all temperatures. Our results show that irradiation provides a "clean" tuning knob for the mean free path, without altering other system parameters. This suggests promising directions for studies of Anderson localization.

DOI: 10.1103/PhysRevMaterials.3.053801

I. INTRODUCTION

A central question in condensed matter physics is the distinction between insulators and metals. In this context, Anderson localization [1–3] and its precursor, weak localization [4,5], are key paradigms that explain how a disordered potential can suppress transport via quantum interference. This is particularly interesting in three spatial dimensions wherein a threshold disorder strength is required to localize electrons. Direct simulations of three-dimensional (3D) Anderson localization have been achieved in areas as diverse as light [6], sound [7], and ultracold atomic gases [8,9]. Signatures of localization have also been seen in solid-state systems, mainly in doped semiconductors [10–13].

In this article, we study localization in rare-earth nickelates by controllably tuning disorder. This family of materials [14] hosts complex phenomena such as non-Fermi-liquid character [15], charge fluctuations [16], and magnetic correlations [17]. Recent studies have shown that nickelate films also host metal-insulator transitions as the film width is tuned [18–20]. We demonstrate a similar transition that is directly driven by disorder, rather than dimensionality.

A key quantity that determines transport in a metal is the mean free path, the average distance traveled by electrons between successive collisions. The collisions themselves can be elastic (between electrons and crystal defects) or inelastic (electron-electron or electron-phonon scattering). We use ion irradiation to induce defects [21–24], thereby directly controlling the elastic-scattering rate. By tuning defect concentration, we find rich transport behavior, going through regimes of Mott-Ioffe-Regel scattering, weak localization, and variable-range hopping. To describe our observations at intermediate disorder strengths, we present a theoretical model generalizing results from weak localization theory from one and two dimensions to three dimensions.

II. EXPERIMENTAL DETAILS

$LaNiO_3$ (LNO) films of width 50 nm were epitaxially grown on $SrTiO_3$ (STO) (001) single crystals ($a_{sub} = 3.905$ Å)

*changan.wang@hzdr.de
†cutygo@phys.ncku.edu.tw

by pulsed laser deposition. The films were then irradiated by 6 keV He ions with four different fluences, $\Phi = (1, 1.75, 2.5, 5) \times 10^{15}$ He cm^{-2}. Low fluence values were chosen to avoid extended defects [25]. During irradiation, the beam was raster scanned to ensure lateral homogeneity. Our work is, in part, motivated by early studies on ternary borides where He irradiation was shown to affect transport [26]. The He ions create point defects with a density that increases with fluence. Helium's nobility ensures that no extra holes or electrons are introduced. It does induce strain that is relieved by an increase of out-of-plane lattice constant (see the Supplemental Material [27]), but this does not significantly affect carrier density. The pristine and irradiated samples were characterized by x-ray diffraction (XRD) (PANalytical X'Pert PRO diffractometer) using Cu $K\alpha$ radiation. Transport properties were measured using a van der Pauw geometry and a constant current source. To measure temperature dependence, temperature was swept at a slow rate of 1–2 K/min with a Lakeshore 332 temperature controller. We have performed the same measurements on $PrNiO_3$ as well, with qualitatively similar results.

III. RESISTIVITY

Metallic and insulating behaviors are distinguished by the temperature dependence of resistivity. Figure 1(a) shows resistivity vs temperature for the pristine film as well as irradiated samples. The pristine film as well that with the lowest fluence are both metallic at all temperatures. In contrast, the sample with the largest fluence ($\Phi = 5 \times 10^{15}$ He cm^{-2}) exhibits insulating behavior at all temperatures. At intermediate fluences, we see a clear minimum in the resistivity, indicating a metal-insulator crossover (MIC). Here, we use the term MIC to denote a thermal crossover where the slope of resistivity vs temperature changes sign. We observe that the MIC temperature increases with increasing fluence.

IV. METALLIC SIDE OF THE MIC

In a typical metal, resistivity increases with temperature according to

$$\rho_{\text{ideal}}(T) = \rho_0 + AT^n. \tag{1}$$

The resistivity at zero temperature, ρ_0, arises due to *elastic* scattering from defects in the crystal—a measure of disorder strength. In contrast, the temperature-dependent contribution arises largely from *inelastic* electron-electron and electron-phonon scattering [28]. In a Fermi liquid, when electron-electron scattering is dominant, the exponent is $n = 2$ leading to a characteristic quadratic behavior. The interplay of elastic and inelastic scattering can be described in terms of the mean free path, ℓ, with $\rho \propto \ell^{-1}$ [29],

$$\frac{1}{\ell} = \frac{1}{\ell_e} + \frac{1}{\ell_{\text{in}}}, \tag{2}$$

as the elastic (ℓ_e) and inelastic (ℓ_{in}) scattering rates combine additively. With increasing temperature, ℓ_{in} decreases, leading

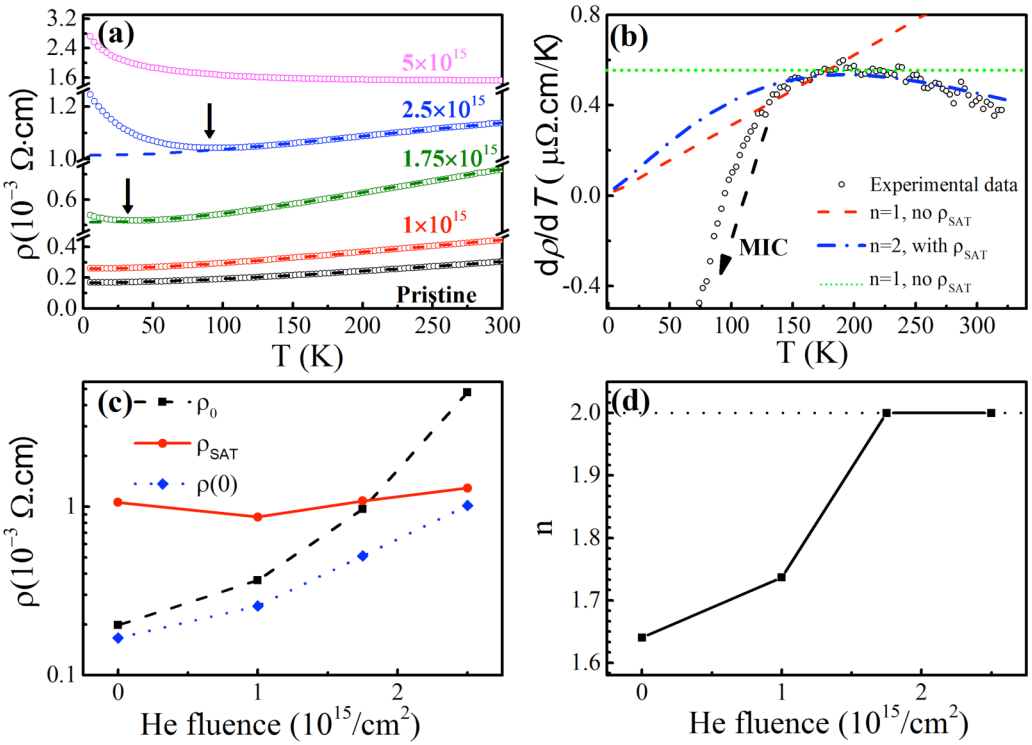

FIG. 1. (a) Resistivity vs temperatures of LNO samples with increasing irradiation fluence. Arrows mark metal-insulator crossovers (MICs). The dashed lines are fits to data in the metallic region using Eqs. (1) and (3). (b) Temperature derivative of the resistivity as a function of temperature for the sample with a fluence $\Phi = 2.5 \times 10^{15}$ He cm^{-2}. The downturn at lower temperature represents the MIC. Red dashed and green dotted lines are fits with $\rho_{\text{sat}} = 0$, which do not describe the data well. (c) ρ_0, ρ_{sat}, and $\rho(T = 0)$ obtained at different fluences. (d) Extracted exponents n for different fluences.

to increasing resistivity. This increase cannot go on indefinitely as the mean free path cannot be shorter than the lattice spacing. The regime when the mean free path is comparable to the lattice spacing is called the Mott-Ioffe-Regel limit [30,31]. This leads to an upper bound on the resistivity, ρ_{sat}, which can be thought of as arising from Heisenberg's uncertainty principle [30,32,33]. The overall resistivity is given by

$$\rho^{-1}(T) = \rho_{ideal}^{-1}(T) + \rho_{sat}^{-1}. \quad (3)$$

This parallel-resistor formula is well known to describe a wide variety of metals [30].

Here, we find that nickelate films on the metallic side of the MIC are well described by a combination of Eqs. (3) and (1). We fit the resistivity data taking ρ_0, ρ_{sat}, A, and n as fitting parameters. The obtained results are shown in Figs. 1(c) and 1(d). In order to obtain a reasonable fit, it is essential to include a saturation resistivity ρ_{sat} using the parallel resistor formula of Eq. (3) [19]. This is brought out in Fig. 1(b), which shows the derivative of resistivity and the corresponding fitting curves. As shown in Fig. 1(c), the resistivity extrapolated to zero temperature, $\rho(0)$, exhibits the typical result of parallel resistor addition. For low fluences, when $\rho_0 \ll \rho_{sat}$, $\rho(0)$ tracks ρ_0. At high fluences, when $\rho_0 \gg \rho_{sat}$, $\rho(0)$ approaches ρ_{sat}.

As shown in Fig. 1(c), ρ_0 increases with fluence—consistent with our expectation that ρ_0 is determined by the density of defects which controls the elastic mean free path. As the change in ρ_0 may also be attributed to changing carrier density, we compared Hall resistivity data on three samples: (i) the pristine, (ii) $\Phi = 1 \times 10^{15}$, and (iii) $\Phi = 1.75 \times 10^{15}$ He cm^{-2} samples at 75 K (all three samples are metallic at this temperature). The densities inferred from the Drude formula [34] are 2.02, 1.40, and 1.31 ($\times 10^{22}$ cm^{-3}), respectively. This shows that changes in transport are driven by changing defect density, rather than carrier density. For example, the $\Phi = 1 \times 10^{15}$ (always metallic) and $\Phi = 1.75 \times 10^{15}$ (hosting an MIC) samples only differ by ~7% in carrier density, but by ~60% in ρ_0.

The saturation resistivity ρ_{sat} is more or less independent of fluence, in line with our expectation that ρ_{sat} is an intrinsic material property that depends on the lattice constant (and perhaps the carrier density). Earlier studies have suggested that ρ_{sat} in nickelate films is sensitive to the in-plane strain [19] as it modifies bands near the Fermi energy [35]. In our samples, the in-plane strain is fixed by the STO substrate and does not vary with irradiation (see the Supplemental Material [27]). Indeed, our ρ_{sat} value is close to that seen in thick $LaNiO_3$ films [19].

The fluence dependence of ρ_0 and ρ_{sat} indicates progression towards the Mott-Ioffe-Regel limit and beyond. We find that ρ_0 exceeds ρ_{sat} at a fluence of $\Phi \approx 1.75 \times 10^{15}$ He cm^{-2}. This suggests that the elastic mean free path becomes comparable to the lattice spacing (we support this assertion with further arguments below). Surprisingly, this is reflected in the exponent n, plotted in Fig. 1(d). For low fluences, the exponent is $n \approx 1.6$ indicating non-Fermi-liquid (NFL) behavior, known to be present in LNO. This could possibly arise from lattice [15], charge [16], or magnetic fluctuations [17,36]. At large fluences with $\Phi \gtrsim 1.75 \times 10^{15}$ He cm^{-2}, we find $n \approx 2$, suggesting Fermi-liquid (FL) character. Remarkably, this NFL-FL transition coincides with the Mott-Ioffe-Regel (MIR) limit as suggested by ρ_0 and ρ_{sat} values. This suggests that a large disorder concentration is required to suppress magnetic or lattice fluctuations. NFL character in the nickelates and in heterostructures has seen a surge of interest with many recent experimental studies [19,37,38]. Our results suggest that this behavior can be tuned by disorder concentration and, indeed, vanishes in the MIR limit.

V. INSULATING SIDE OF THE MIC

Having discussed the MIC seen at intermediate fluence values ($\Phi = 1.75 \times 10^{15}$ and 2.5×10^{15} He cm^{-2}), we characterize the insulating side of the crossover. In three dimensions, a threshold disorder strength is required to bring about Anderson localization. Below this threshold, quantum interference effects may increase resistivity [39,40]. We argue that this "weak localization" phenomenon is the underlying reason behind the minimum in resistivity at the MIC. On the insulating side, assuming diffusive transport and long inelastic-scattering times, we show that resistivity can be described by (see the Supplemental Material [27])

$$\rho(T) = \rho(0) - \alpha T^{n/2} + \beta T^{n} - \gamma T^{3n/2}, \quad (4)$$

where α, β, and γ are coefficients related to the ratio of inelastic and elastic mean free paths, ℓ_{in}/ℓ_e,

$$\frac{\ell_{in}(T)}{\ell_e} = \frac{1}{\pi}\left(\frac{\beta^2}{\alpha^2} - \frac{\gamma}{\alpha}\right)^{-1} T^{-n}. \quad (5)$$

In Fig. 2(a), the resistivity is shown with the best fit to Eq. (4).

We obtain an excellent fit for our data with $n = 1.5$, indicating that the inelastic-scattering process is dominated by electron-electron interactions. In a clean metal, electron-electron interactions lead to $\ell_{in} \propto T^{-2}$ [28,41]. However, disorder scattering in three dimensions modifies this to $\ell_{in} \propto T^{-3/2}$ [42–44]. In contrast, electron-phonon scattering gives rise to $\ell_{in} \propto T^{-3}$ [45].

The ratio ℓ_{in}/ℓ_e of Eq. (5), obtained from best fit parameters, is shown in Fig. 2(b). The increase of He fluence from $\Phi = 1.75 \times 10^{15}$ to 2.5×10^{15} He cm^{-2} increases defect

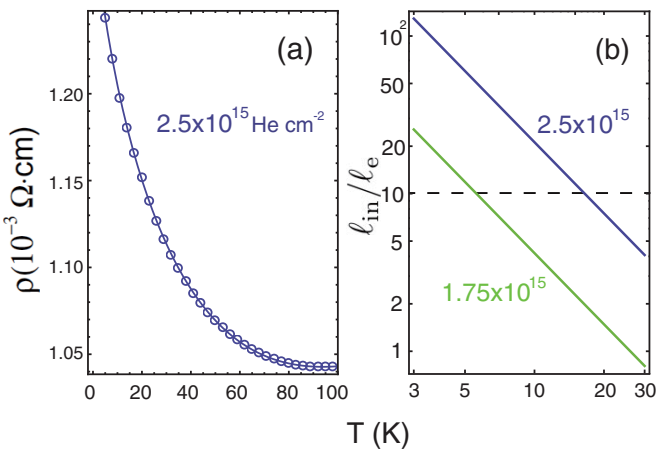

FIG. 2. (a) Increase of resistivity on the insulating side of the MIC, with a fit to Eq. (4). (b) A log-log plot of the ratio of mean free paths, obtained from the fitting parameters using Eq. (5).

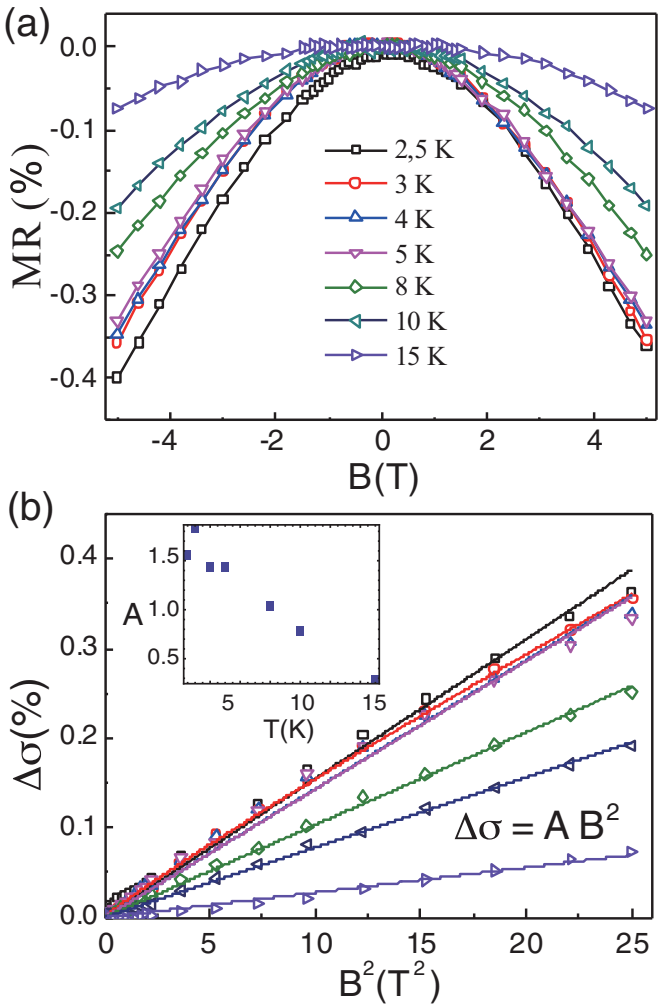

FIG. 3. (a) Magnetoresistance ($\{R(H) - R(0)\}/R(0)$) vs field in the LNO sample irradiated with fluence 2.5×10^{15} He cm^{-2} at different temperatures. (b) Fractional increase in magnetoconductivity ($\Delta\sigma(\%) = \{\sigma(B) - \sigma(0)\}/\sigma(0)$) vs the square of the magnetic field. The inset shows the fitting parameter A (units 10^{-4} T^{-2}) as a function of temperature.

concentration, thereby decreasing ℓ_e and increasing $\ell_{\rm in}/\ell_e$. The obtained ratio $\ell_{\rm in}/\ell_{\rm e}$ allows us to make quantitative statements about approaching the MIR limit. For instance, in the sample with $\Phi = 2.5 \times 10^{15}$ He cm^{-2} with temperature $\sim$3 K, we find $\ell_{\rm in}/\ell_{\rm e} \gtrsim 100$ as shown in Fig. 2(b). In this temperature range, the inelastic mean free path ($\ell_{\rm in}$) for an LNO film is known to be approximately 40 nm [18,46]. Therefore, the elastic mean free path ($\ell_{\rm e}$) is as short as 4 Å, close to the LNO lattice constant 3.83 Å. This confirms that the film is indeed at the MIR limit. From the large value of $\ell_{\rm in}/\ell_{\rm e}$, we also deduce that inelastic-scattering processes are weak at low temperatures. This leads to long coherence times, while transport remains diffusive as elastic scattering is not strong enough to localize carriers. This allows for quantum interference effects captured by our weak localization analysis.

To further characterize the insulating side of the MIC, we present magnetotransport data. Figure 3(a) shows magnetoresistance (MR) at different temperatures for the sample irradiated with fluence $\Phi = 2.5 \times 10^{15}$ He cm^{-2}. From the above discussion, this sample is expected to be close to the MIR limit. Resistance decreases with B, the applied magnetic field, as time-reversal breaking disrupts quantum interference effects that are responsible for weak localization. In our samples that lie in the MIR regime, the elastic mean free path is a few angstroms. The magnetic length, however, is $\ell_B \approx 26/\sqrt{B\,(\rm T)}$ nm, which is always much greater than ℓ_e. In this regime, with $\ell_B \gg \sqrt{\ell_e \ell_{\rm in}}$, the magnetoconductivity scales as [47]

$$\Delta\sigma(\%) = \frac{\sigma(B,T)}{\sigma(0,T)} - 1 \approx \left(\frac{\ell_{\rm in}}{\ell_{\rm e}}\right)^{3/2} \left(\frac{e\tau_{\rm e}}{m^\star}\right)^2 B^2, \qquad (6)$$

where $m^\star$ is the electron effective mass and $\tau_{\rm e} = \ell_{\rm e}/v_F$ is the elastic relaxation time. Our data are in good agreement with this form as shown in Fig. 3(b); we see that B^2 scaling persists over a large field range, up to 5 T. Moreover, the fitting parameter A in Fig. 3(b) decreases with the increase of temperature. This is consistent with Eq. (6) as the ratio $\ell_{\rm in}/\ell_e$ decreases with temperature [see Fig. 2(b)]. The magnetoconductivity of the sample irradiated with fluence $\Phi = 1.75 \times 10^{15}$ He cm^{-2} also shows B^2 scaling, as do our irradiated $PrNiO_3$ samples (see the Supplemental Material [27]). In pristine LNO, with a field of several tesla, the magnetoconductivity scales as $B^{1/2}$ as the mean free path is longer than the magnetic length [46]. The observation of B^2 behavior in our samples provides strong evidence for 3D weak localization. In earlier studies, this behavior was only seen for $B \lesssim 1$ T [48] as it is only expected to hold for $B \ll B_c \approx (\hbar c/e)/(\ell_{\rm in}\ell_e)$. We see this regime for a larger field range as the ultrashort elastic mean free path leads to a large B_c value.

VI. INSULATING SAMPLES

Having discussed both sides of the MIC seen at intermediate fluence, we discuss the sample with highest fluence, $\Phi = 5 \times 10^{15}$ He cm^{-2} [see Fig. 1(a)]. This shows insulating behavior at all temperatures. With high disorder concentration, we expect electrons to be Anderson localized. Transport can only occur via hopping between localized states that are well separated in position and energy, equivalent to a percolation process [49]. In this scenario, resistivity follows the variable range hopping (VRH) paradigm [50], with

$$\rho(T) = C\exp(T_0/T)^{1/(1+d)}, \qquad (7)$$

where d is the number of spatial dimensions. T_0 is a constant that depends on both the density of localized states and the spatial decay profiles of wave functions. Figure 4 shows our resistivity data with a fit to Eq. (7) with $d = 3$. We obtain a good fit from 10 to 100 K. Earlier studies on ultrathin LNO films that are insulating have shown good agreement with VRH behavior, described by Eq. (7) with $d = 2$ [18,51]. The two-dimensionality arises from lateral confinement [52,53]. Here, as our film thickness is 50 nm, much greater than the mean free path, we find three-dimensional character.

VII. DISCUSSION

We have studied transport in nickelate films, with tunable disorder. With irradiation as a tuning knob, we see (i) a metallic phase in the clean regime, (ii) metal-insulator crossovers

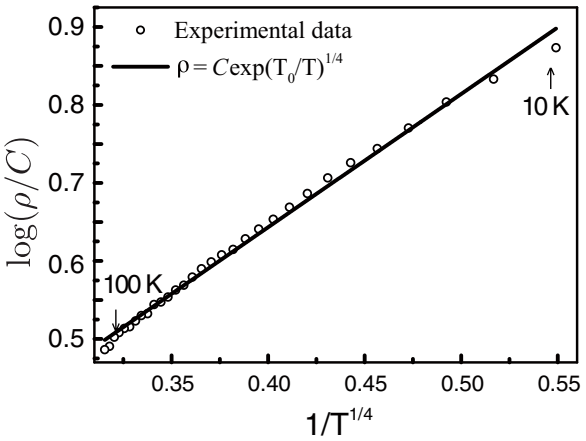

FIG. 4. Logarithm of resistivity vs $T^{-1/4}$ for the sample irradiated with fluence 5×10^{15} He cm^{-2}. The black line is a fit to the data between 10 and 100 K.

for intermediate disorder, and (iii) insulating behavior for high disorder. Our results in $LaNiO_3$ are robust, with the same qualitative results occurring in irradiated $PrNiO_3$ [54] (see the Supplemental Material [27]). They can be compared with earlier studies on the nickelates using various tuning parameters: electric fields [55], oxygen vacancies [15], strain [19], and film thickness [18,56]. We argue that irradiation provides a superior tuning knob as it changes only the elastic mean free path, without strongly affecting carrier density, dimensionality, or band energies (see the Supplemental Material [27]). It is also highly suitable for practical applications as it is chip-technology compatible and can be adapted for large-scale production. Previous studies have shown that irradiation can affect transport in nickelate films [57–59]. Our study builds on these by demonstrating the full range of localization phenomena in three dimensions.

Irradiated nickelates open a new window for the study of Anderson localization, as they allow for a clean handle on the mean free path. In particular, the following exciting question arises: Can we detect a "mobility edge" [60,61] in a solid-state system? In our samples with intermediate disorder, a new temperature scale (associated with the MIC) emerges. Measurements such as optical conductivity could reveal whether this is correlated with a mobility edge in the electronic spectrum. Such measurements are of great interest in the context of recent ultracold-atom experiments [62,63].

ACKNOWLEDGMENTS

We thank A. Möbius for critical feedback on the manuscript. C.W. is thankful for financial support from the China Scholarship Council (Grant No. 201606750007). C.-H.C. and P. P. acknowledge financial support from the German Research Foundation (Deutsche Forschungsgemeinschaft, Grants No. CH 2051/1-1 and No. ZH 225/6-1.). C.-H.C. and Y.H.C. acknowledge financial support from the Ministry of Science and Technology, Taiwan (Grants No. 107-2112-M-006-025-MY3 and No. 107-2923-M-009-005-MY3). C.-H.C. acknowledges support from the Ministry of Education, Taiwan. C.-H.C., A.H., and H.-T.J. acknowledge support from the National Center for Theoretical Sciences. R.G. thanks IFW Dresden for hospitality.

C.W. and C.-H.C. contributed equally to this work.

[1] P. W. Anderson, Phys. Rev. **109**, 1492 (1958).
[2] P. A. Lee and T. V. Ramakrishnan, Rev. Mod. Phys. **57**, 287 (1985).
[3] B. Kramer and A. MacKinnon, Rep. Prog. Phys. **56**, 1469 (1993).
[4] S. Chakravarty and A. Schmid, Phys. Rep. **140**, 193 (1986).
[5] C. W. J. Beenakker and H. van Houten, Phys. Rev. B **38**, 3232 (1988).
[6] D. S. Wiersma, P. Bartolini, A. Lagendijk, and R. Righini, Nature (London) **390**, 671 (1997).
[7] H. Hu, A. Strybulevych, J. H. Page, S. E. Skipetrov, and B. A. van Tiggelen, Nat. Phys. **4**, 945 (2008).
[8] S. S. Kondov, W. R. McGehee, J. J. Zirbel, and B. DeMarco, Science **334**, 66 (2011).
[9] F. Jendrzejewski, A. Bernard, K. Müller, P. Cheinet, V. Josse, M. Piraud, L. Pezzé, L. Sanchez-Palencia, A. Aspect, and P. Bouyer, Nat. Phys. **8**, 398 (2012).
[10] S. Katsumoto, F. Komori, N. Sano, and S. ichi Kobayashi, J. Phys. Soc. Jpn. **56**, 2259 (1987).
[11] S. Waffenschmidt, C. Pfleiderer, and H. v. Löhneysen, Phys. Rev. Lett. **83**, 3005 (1999).
[12] K. M. Itoh, M. Watanabe, Y. Ootuka, E. E. Haller, and T. Ohtsuki, J. Phys. Soc. Jpn. **73**, 173 (2004).
[13] A. Möbius, Crit. Rev. Solid State Mater. Sci. **0**, 1 (2018).
[14] M. L. Medarde, J. Phys. Condens. Matter **9**, 1679 (1997).
[15] R. Jaramillo, S. D. Ha, D. M. Silevitch, and S. Ramanathan, Nat. Phys. **10**, 304 (2014).
[16] S. Johnston, A. Mukherjee, I. Elfimov, M. Berciu, and G. A. Sawatzky, Phys. Rev. Lett. **112**, 106404 (2014).
[17] H. Guo, Z. W. Li, L. Zhao, Z. Hu, C. F. Chang, C. Y. Kuo, W. Schmidt, A. Piovano, T. W. Pi, O. Sobolev *et al.*, Nat. Commun. **9**, 43 (2018).
[18] R. Scherwitzl, S. Gariglio, M. Gabay, P. Zubko, M. Gibert, and J.-M. Triscone, Phys. Rev. Lett. **106**, 246403 (2011).
[19] E. Mikheev, A. J. Hauser, B. Himmetoglu, N. E. Moreno, A. Janotti, C. G. Van de Walle, and S. Stemmer, Sci. Adv. **1**, e1500797 (2015).
[20] H. Wei, M. Jenderka, M. Bonholzer, M. Grundmann, and M. Lorenz, Appl. Phys. Lett. **106**, 042103 (2015).
[21] J. P. Rivière, *Application of Particle and Laser Beams in Materials Technology*, Nato Science Ser. E Vol. 283 (Springer, Berlin, 1995).
[22] T. D. de la Rubia, Annu. Rev. Mater. Sci. **26**, 613 (1996).
[23] A. V. Krasheninnikov and K. Nordlund, J. Appl. Phys. **107**, 071301 (2010).
[24] H. Guo, S. Dong, P. D. Rack, J. D. Budai, C. Beekman, Z. Gai, W. Siemons, C. M. Gonzalez, R. Timilsina, A. T. Wong, A. Herklotz, P. C. Snijders, E. Dagotto, and T. Z. Ward, Phys. Rev. Lett. **114**, 256801 (2015).

[25] R. Livengood, S. Tan, Y. Greenzweig, J. Notte, and S. McVey, J. Vac. Sci. Technol. **27**, 3244 (2009).

[26] J. Rowell, R. Dynes, and P. Schmidt, in *Superconductivity in D- and F-Band Metals*, edited by H. Suhl and M. B. Maple (Academic Press, New York, 1980), pp. 409–418.

[27] See Supplemental Material at http://link.aps.org/supplemental/10.1103/PhysRevMaterials.3.053801 for the XRD data of LNO films, the derivation of the resistivity formula, the transport data for the sample with fluence $\Phi = 1.75 \times 10^{15}$ He cm^{-2}, the measurement of $PrNiO_3$ samples, and the first-principles calculations by using density functional theory [64-71].

[28] G. F. Giuliani and J. J. Quinn, Phys. Rev. B **26**, 4421 (1982).

[29] C. W. J. Beenakker and H. van Houten, Solid State Phys. **44**, 1 (1991).

[30] O. Gunnarsson, M. Calandra, and J. E. Han, Rev. Mod. Phys. **75**, 1085 (2003).

[31] N. E. Hussey, K. Takenaka, and H. Takagi, Philos. Mag. **84**, 2847 (2004).

[32] H. Wiesmann, M. Gurvitch, H. Lutz, A. Ghosh, B. Schwarz, M. Strongin, P. B. Allen, and J. W. Halley, Phys. Rev. Lett. **38**, 782 (1977).

[33] M. Gurvitch, Phys. Rev. B **24**, 7404 (1981).

[34] N. Ashcroft and N. Mermin, *Solid State Physics* (Holt, Rinehart and Winston, New York, 1976).

[35] H. K. Yoo, S. I. Hyun, L. Moreschini, H.-D. Kim, Y. J. Chang, C. H. Sohn, D. W. Jeong, S. Sinn, Y. S. Kim, A. Bostwick *et al.*, Sci. Rep. **5**, 8746 (2015).

[36] A. Subedi, SciPost Phys. **5**, 020 (2018).

[37] J. Y. Zhang, H. Kim, E. Mikheev, A. J. Hauser, and S. Stemmer, Sci. Rep. **6**, 23652 (2016).

[38] V. E. Phanindra, P. Agarwal, and D. S. Rana, Phys. Rev. Mater. **2**, 015001 (2018).

[39] B. L. Al'tshuler, A. G. Aronov, A. I. Larkin, and D. E. Khmel'nitskii, Sov. Phys. JETP **54**, 411 (1981).

[40] David V. Baxter, R. Richter, M. L. Trudeau, R. W. Cochrane, and J. O. Strom-Olsen, J. Phys. France **50**, 1673 (1989).

[41] W. G. Baber, Proc. R. Soc. London A **158**, 383 (1937).

[42] A. Schmid, Z. Phys. **271**, 251 (1974).

[43] B. L. Al'tshuler and A. G. Aronov, JETP Lett. **2**, 482 (1979).

[44] C. Y. Wu and J. J. Lin, Phys. Rev. B **50**, 385 (1994).

[45] J. Rammer and A. Schmid, Phys. Rev. B **34**, 1352 (1986).

[46] G. Herranz, F. Sánchez, J. Fontcuberta, V. Laukhin, J. Galibert, M. V. García-Cuenca, C. Ferrater, and M. Varela, Phys. Rev. B **72**, 014457 (2005).

[47] A. Kawabata, Solid State Commun. **34**, 431 (1980).

[48] Y. G. Arapov, G. I. Harus, V. N. Neverov, N. G. Shelushinina, and O. A. Kuznetsov, Semiconductors **33**, 978 (1999).

[49] N. Apsley and H. P. Hughes, Philos. Mag. **31**, 1327 (1975).

[50] N. F. Mott, Philos. Mag. **19**, 835 (1969).

[51] W. Brenig, G. H. Döhler, and H. Heyszenau, Philos. Mag. **27**, 1093 (1973).

[52] C. Ortix, S. Kiravittaya, O. G. Schmidt, and J. van den Brink, Phys. Rev. B **84**, 045438 (2011).

[53] C.-H. Chang and C. Ortix, Int. J. Mod. Phys. B **31**, 1630016 (2017).

[54] M. Hepting, M. Minola, A. Frano, G. Cristiani, G. Logvenov, E. Schierle, M. Wu, M. Bluschke, E. Weschke, H.-U. Habermeier, E. Benckiser, M. Le Tacon, and B. Keimer, Phys. Rev. Lett. **113**, 227206 (2014).

[55] R. Scherwitzl, P. Zubko, C. Lichtensteiger, and J.-M. Triscone, Appl. Phys. Lett. **95**, 222114 (2009).

[56] D. S. L. Pontes, F. M. Pontes, M. A. Pereira-da Silva, O. M. Berengue, A. J. Chiquito, and E. Longo, MRS Online Proc. Libr. **1633**, 25 (2014).

[57] Y. Kumar, A. Pratap Singh, S. K. Sharma, R. J. Choudhary, P. Thakur, M. Knobel, N. B. Brookes, and R. Kumar, Appl. Phys. Lett. **101**, 112103 (2012).

[58] Y. Kumar, R. J. Choudhary, and R. Kumar, J. Appl. Phys. **120**, 115306 (2016).

[59] Y. Kumar, H. Bhatt, C. L. Prajapat, H. K. Poswal, S. Basu, and S. Singh, J. Appl. Phys. **124**, 065302 (2018).

[60] N. Mott and E. Davis, *Electronic Processes in Non-crystalline Materials* (Oxford University Press, Oxford, 2012).

[61] N. Mott, J. Phys. C **20**, 3075 (1987).

[62] G. Semeghini, M. Landini, P. Castilho, S. Roy, G. Spagnolli, A. Trenkwalder, M. Fattori, M. Inguscio, and G. Modugno, Nat. Phys. **11**, 554 (2015).

[63] M. Pasek, G. Orso, and D. Delande, Phys. Rev. Lett. **118**, 170403 (2017).

[64] G. Kresse and J. Hafner, Phys. Rev. B **48**, 13115 (1993).

[65] G. Kresse and J. Furthmüller, Comput. Mater. Sci. **6**, 15 (1996).

[66] G. Kresse and J. Furthmüller, Phys. Rev. B **54**, 11169 (1996).

[67] G. Kresse and D. Joubert, Phys. Rev. B **59**, 1758 (1999).

[68] P. E. Blöchl, Phys. Rev. B **50**, 17953 (1994).

[69] J. P. Perdew, K. Burke, and M. Ernzerhof, Phys. Rev. Lett. **77**, 3865 (1996).

[70] A. I. Liechtenstein, V. I. Anisimov, and J. Zaanen, Phys. Rev. B **52**, R5467 (1995).

[71] J. L. García-Muñoz, J. Rodríguez-Carvajal, P. Lacorre, and J. B. Torrance, Phys. Rev. B **46**, 4414 (1992).